Journal of Electrostatics 94 (2018) 51–59

Contents lists available at ScienceDirect

Journal of Electrostatics

journal homepage: www.elsevier.com/locate/elstat

Characterizations of solid-liquid interface in a wet-mate subsea HVDC connector

Mattewos Tefferi[a,b], Mona Ghassemi[b], Christopher Calebrese[c], Qin Chen[c], Yang Cao[a,b,*]

[a] Electrical and Computer Engineering, University of Connecticut, 371 Fairfield Way, Storrs, CT 06269, USA
[b] Electrical Insulation Research Center, Institute of Materials Science, University of Connecticut, 97 North Eagleville Road, Storrs, CT 06269, USA
[c] GE Global Research Center, Niskayuna, NY 12309, USA

ARTICLE INFO

Keywords:
HVDC
Wet-mate connector
Subsea
Kerr electro-optics
Conduction
Solid-liquid interface
Space charge

ABSTRACT

Wet-mate connectors represent essential and technically challenging components in a subsea HVDC system. In this paper, systematic characterizations of solid-liquid insulation system implemented in a Wet-Mate subsea connector are presented with special focus on the interfaces. First, conduction in the liquid gap was studied using the current-voltage characterization and the Kerr electro-optic field mapping to establish the correlation between conduction and DC field grading for various electrode gap configurations and oil types. Secondly, Kerr electro-optic field sensing was extended to solid-liquid interfaces for model Wet-Mate connectors. Studies suggest that DC field grading in solid-liquid insulation particularly along the interface is influenced by regimes of conduction depending on the electrode configuration, gap separation, polarity, oil type, moisture and contaminants, and such dependences are further affected by the DC properties of hybrid solid-liquid insulations. Exemplar modelling studies conducted on representative design configurations indicate that this comprehensive basic study could provide insight into the tailoring of solid-liquid interfaces with low field distortion under quasi steady-state and polarity reversal operations for safe design and optimization of DC Wet-Mate connectors.

1. Introduction

Oil and gas (O&G) industries are undergoing a transformation from reservoirs in existing brownfield sites to offshore drilling activities located in deeper water. For technical and economic reasons, processing of hydrocarbons is preferred on the seabed in Ultra Deep-Water (UDW) sites instead of doing it on a host platform at the surface. As a result, O&G industries are continuously seeking new technologies for accessing deep sea petroleum resources. Subsea DC transmission and distribution system is a promising technology for electrifying subsea O&G production with high power, long distance and UDW depth [1,2].

For subsea DC power system such as the Modular Stacked Direct Current (MSDC) system, Dry-Mate (DM) and Wet-Mate (WM) connectors are essential components for system field deployment, faulty component isolation and repairing. Currently, there are commercially available DM and WM AC connectors, such as GE Vetco Gray MECON™ with a rating of 36 kV/500 A for operation in a depth of 3048 m [3]. Technical challenges of DC WM connectors include those related to DC systems as well as subsea installation and operation [1,2,4,5]. Comparing to existing subsea AC connectors, a subsea DC connector would require different electrical insulation system due to significant difference between AC and DC electric field grading. In AC system, the electric field is capacitive graded, i.e., determined by dielectric permittivity, which is nearly independent of the field and temperature. On the other hand, for DC system, the field is resistively graded, i.e., determined by electrical conductivity, which has strong nonlinear field- and temperature-dependence. In addition, the effect of space charge poses another challenge for DC insulation. Under DC voltage, with the presence of an interface between different materials, electrical charges migrate and accumulate therein to form space charges that can significantly alter the field distribution. Furthermore, during fault transients and polarity reversal events, superimpose of AC and DC field components results in an exceedingly high electric field. Therefore, DC connectors must also be designed to operate reliably for ont only capacitive grading, but also resistive grading, and a combination of resistive and capacitove grading [4,5].

WM connectors will be installed remotely at the rated water depth, with the interior of the WM chamber exposed to seawater during the mating process. Their electrical insulation must be reliably established after the mating is finished. Under these remote and harsh environment conditions, servicing of equipment is restricted, and reliability is of utmost importance. However, the dielectric strength of the insulating

* Corresponding author. Electrical and Computer Engineering, Institute of Materials Science, University of Connecticut, 97 North Eagleville Road, Storrs, CT 06269, USA.
E-mail address: yang.cao@uconn.edu (Y. Cao).

https://doi.org/10.1016/j.elstat.2018.06.001
Received 26 April 2018; Received in revised form 9 June 2018; Accepted 9 June 2018

material is highly sensitive to contaminations. For DC insulation in particular, the contaminants can affect the conductivity and charge distribution of the material, which in turn affect the DC field distribution. Special insulation designs and material formulation have been developed specifically for cables and cable accessories in HVDC transmission and distribution system and have undergone significant progress in recent years. However, due to the requirement of subsea installation, certain contamination may be unavoidable. For example, in a WM connector, the interior of WM chamber must be exposed to seawater during the mating process, and afterward, the electrical insulation performance is re-established. Even with specially developed rinsing, flushing techniques, remnant contaminants could still present in the insulation after wet-mating. To achieve high reliability of DC WM connectors, it is important to understand the impact of seawater-related contamination on DC insulation [5].

Solid-liquid insulation systems employed for converter transformers have been extensively studied [6]. Certain common features are shared by converter transformer and WM connector hybrid insulation systems. For instance, the conductivity of oil is typically one to two orders of magnitude higher than solids, and hence under DC steady state the electrical stress almost completely lies in the solid insulation. However, the insulation system of a converter transformer is different from that in a WM connector. First, the insulation materials used in a converter transformer are different from those in a WM connector. Pressboard-transformer oil insulation system is most commonly used in converter transformers while WM connectors under study rely on epoxy/rubber and synthetic ester oils insulation. Secondly, during the operation of a WM connector, there are inevitable moisture and seawater contaminants in the mating chamber while converter transformers are manufactured with well-established vacuum drying and baking processes.

For WM DC connectors, oil is an integrated part of the insulation system and provides one of the two barriers in the hybrid insulation structure (Fig. 1). The reliability of oil insulation is highly important. In a proper WM DC connector design, most of the field stress is distributed in solid insulation. However, under transients due to high voltage fault, the stress in oil and along the oil-solid interface can be very high. Therefore, in order to design reliable insulation systems for WM DC connectors, it is important that the behaviours of the DC stressed liquid, solid-liquid interface as well as the effects of marine environment are fully characterized.

In this paper, a comprehensive study was conducted to determine the materials and interface properties that are critical for WM DC operation. The type of materials and interfaces under investigation include: oil insulation, solid-liquid interface, with the consideration for the effects of moisture and salt contaminations. The characterizations include current-voltage measurement and Kerr electro-optical field mapping for oil gaps and along oil-solid interfaces, with barrier layers.

2. Experimental investigation

2.1. Current-voltage characteristics

The investigation of the influence of electrode gap and purity of the oil on the conduction current was carried out by monitoring the quasi steady-state conduction current with a Keithley picoAmp meter for samples subjected to DC bias provided by a Spellman high voltage DC supply. The test cell containing two circular brass electrodes was filled with ~500 mL of oil and kept in dry and clean laboratory conditions. All measurements were conducted at room temperature and atmospheric pressure.

2.2. Kerr electro-optics set up

The Kerr electro-optic measurement system was developed to probe the electric field distribution in liquid insulator as shown schematically in Fig. 2. This oil field sensing method is based on transverse spatial electro-optic modulation, where a phase retardation is developed between lights polarized in parallel and perpendicular to the applied field as the result of Kerr quadratic electro-optic effect [7,8]. In considering the ultra-small Kerr constant of synthetic ester oil used in this study ($7.56 \times 10^{-16}\, m/V^2$), a small AC voltage (200 V, 1 kHz) is superimposed

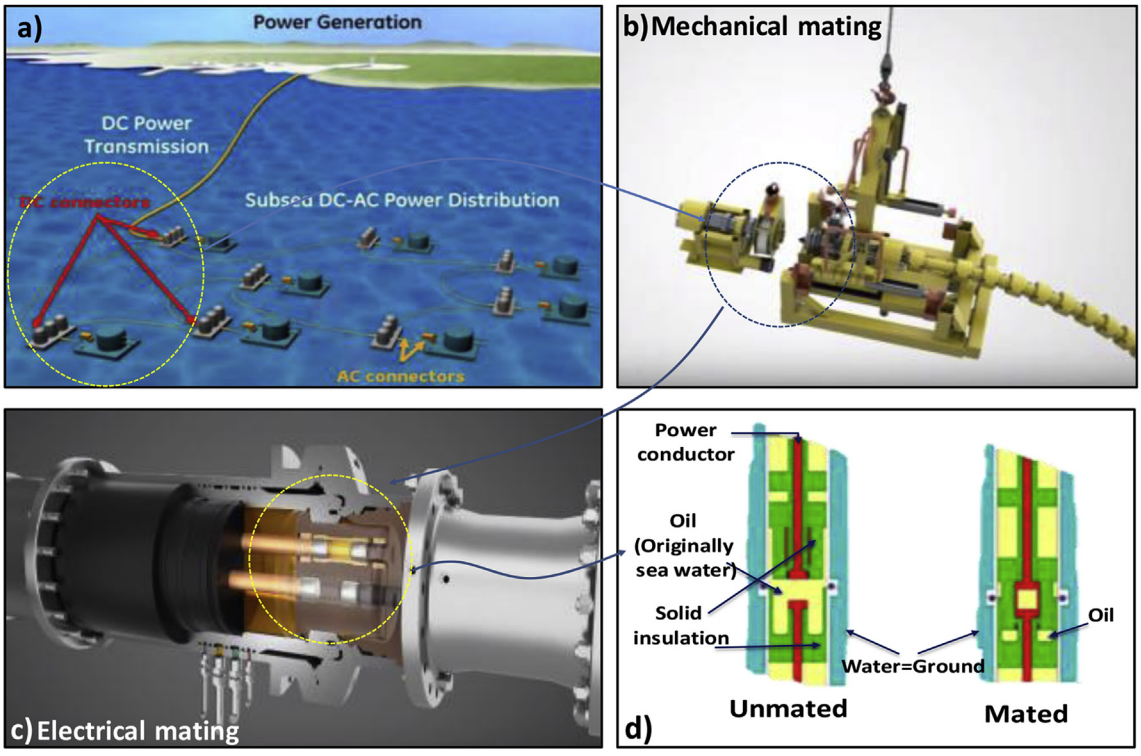

Fig. 1. DC WM connectors used in subsea O&G processing.

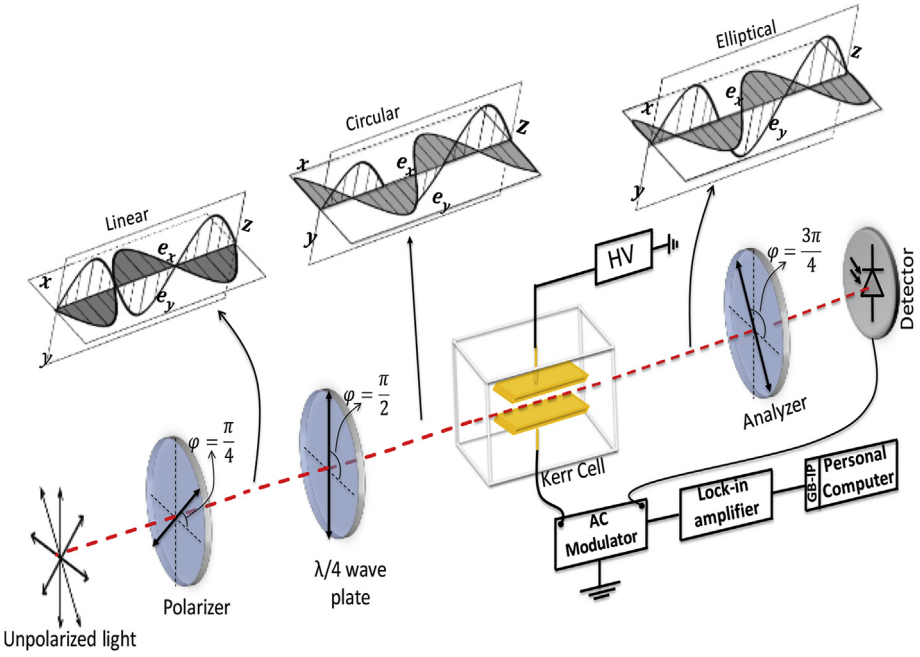

Fig. 2. Kerr electro-optics set up.

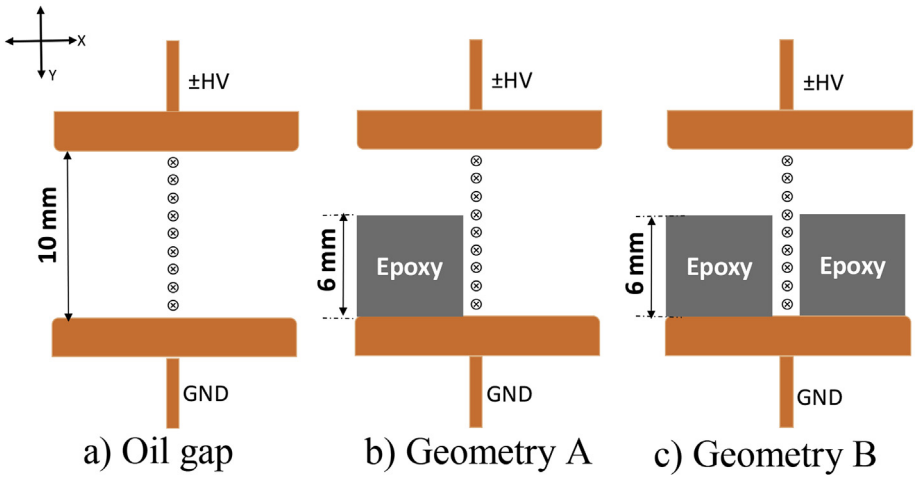

Fig. 3. The geometries under study marked with the path for Kerr electro-optic field intensity measurement.

on the applied DC voltage for Lock-in amplification to enhance the measurement sensitivity. The phase difference ($\Delta\theta$) caused by Kerr effect can be described by Refs. [9,10],

$$\Delta\theta = \frac{I_{1\omega}}{I_{dc}} = 4\pi B L E_{ac} E_{dc} \quad (1)$$

where $I_{1\omega}$ is the first harmonic of light intensity, I_{dc} is the dc component of light intensity, B is the Kerr constant and L is the electrode length. E_{dc} and E_{ac} are the applied DC electric field and superimposed AC electric field, respectively.

2.3. Sample preparation

2.3.1. Solid insulation

The solid dielectric samples were fabricated with commercially available Bisphenol-A based 2-part epoxy containing 61.5 wt% silica fillers. The solid samples are 2 mm, 4 mm or 6 mm in thickness and 10 cm in length. All samples were polished with sand paper and then cleaned and dried thoroughly. The room temperature relative permittivity and electrical conductivity of the epoxy samples are 4.2 and 1.03×10^{-14} S/m, respectively.

2.3.2. Liquid insulation

During the wet-mating operation, the interior insulation of a WM chamber is exposed to seawater. Even with successive flushing of the WM chamber sequentially with deionized water, alcohol and dielectric fluids, remnant contaminations could still exist in the insulation, resulting in the presence of moisture and ions in oil during normal operation. Therefore, to achieve highly reliable operation of DC WM connectors, it is important to understand the impact of seawater-related contaminants on DC insulation. The effect of moisture and ionic contaminants on the field distribution was studied by including three oil samples with controlled contaminants. Oil A is a fresh synthetic ester oil degassed and filtered for at least 24 h. Oil B was prepared by introducing deionized water at 740 ppm to oil A. Oil C was prepared by introducing 200 ppm instant ocean water containing dissolved salt (Na^+, Cl^-) as well as other minor ionic species such as Mg^{++} and SO_4^{--}. The experimental procedure for introducing different levels of moisture and

Table 1
Current density at different conduction regimes.

Conduction Regime	Current density	Creation of charge carriers
Ohmic	$\mathbf{J_0 = \sigma_0 E\sqrt{F(b)}}$ · $F(E) = \frac{I_1(4b)}{2b}$ · $b = \sqrt{\frac{q^3 E}{16\pi\varepsilon_0\varepsilon_r k_B^2 T^2}}$	Dissociation and recombination $A^+B^- \underset{k_r}{\overset{k_D}{\rightleftarrows}} A^+ + B^-$
Saturation	$\mathbf{J_s = k_D(E)qcd}$ · $k_D(E) = k_D^0 F(E)$ · $k_D^0 = k_R \frac{n_0^2}{c}$ · $k_R = \frac{q(\mu_+ + \mu_-)}{\varepsilon_0\varepsilon_r}$	Rarely observed in experiments as injection typically starts to take place.
Injection	$\mathbf{J_i = \mu q_i E_{inj}}$ · $q_i = \frac{Aq_0}{2bK_1(b)}$	Injection of charge carriers $A^+B^-_{interface} \rightarrow A^+/B^-_{free}$

ionic contaminants into oils B and C has been described in Refs. [7,8].

2.3.3. Solid-liquid interface

The essential aspects of solid-liquid interface of the envisaged DC WM connector (Fig. 1d) were studied using two simplified model geometries shown in Fig. 3b and 3c. The geometry A shown in Fig. 3b contains an epoxy plaque having a thickness of 6 mm with an oil gap sandwiched at the midpoint between two electrodes. The geometry B shown in Fig. 3c consists of two epoxy plaques with an oil channel between them. The quasi steady-state electric field intensity under DC is probed by Kerr electro-optics at marked locations shown in Fig. 3.

3. Experimental result and analysis

3.1. Current-voltage characteristics

For nonpolar or weakly polar insulating oils under moderate quasi steady-state fields, charge carriers are mainly created from two sources, i.e., dissociation of ionic pairs in the bulk and "injection" through electrodes [11]. Table 1 summaries the conduction regimes with corresponding governing equations [12–15], where σ_0 is the low field conductivity, E is the electric field strength, k_B is the Boltzmann constant, T is the absolute temperature, q is magnitude of electronic charge, μ_+, μ_- are the mobility of positive and negative ions, $\varepsilon_0 = 8.85 \times 10^{-12} F/m$, ε_r is the relative permittivity, K_D^0 is the dissociation constant at thermodynamic equilibrium, F(E) is field enhancement function, I_1 is the modified Bessel function of the first kind, d is the distance between the electrodes, q_0 is charge in the bulk and K_1 is the modified Bessel function of the second kind.

The current-voltage characteristics for most liquid dielectrics share certain similarities with the ones obtained in gaseous dielectrics, typically with three distinct regions. At low electric fields, the current appears to be a linear function of the applied voltage obeying Ohm's law. At intermediate fields, there is a sub-ohmic region where the current tends to saturate and at high fields the current increases rapidly until breakdown takes place. The saturation region is always presented in gases. However, in dielectric liquids of high resistivity, the saturated current is often overshadowed by the injection current thus in a real experiment, saturation is rarely observed [16,17]. The transition from Ohmic to saturation region occurs when $J_0 = J_s$ and the onset voltage for saturation is given by Ref. [12],

$$V_s = \frac{\sigma_0 d^2 \sqrt{F(b)}}{(\mu_+ + \mu_-)\varepsilon_0\varepsilon_r} \quad (2)$$

The total current density can be separated into two distinct contributions, i.e. the dissociation current and injection current. At low field ($V<V_s$), dissociation current will be the major source of conduction while at high field ($V>V_s$) the injected current dominates. In the bulk of the fluid, the distinction between these two is not possible because injection charge carriers may recombine with the anions generated by dissociation. However, one can distinguish whether dissociation or injection current is dominant based on the fact that the dissociation current density is proportional to the field-enhanced dissociation while the injected current is proportional to the injected charge density at a given field. The nature of the conduction can be determined by which component dominates. Since both components are field dependent, the voltage V_s can be considered as a boundary between two conduction regimes.

Table 2
Conductivity and saturation voltage ($\mathbf{V_s}$) for samples under test.

Oil type	Conductivity	Saturation Voltage V_s	
		10 mm gap	20 mm gap
A	6×10^{-11} S/m	1.2 kV	5.0 kV
B	10×10^{-11} S/m	1.4 kV	7.5 kV
C	13×10^{-11} S/m	2.0 kV	10 kV

The saturation voltage V_s is dependent on the conductivity and electrode separation. A well-accepted value for ionic mobility in synthetic ester oil is $10^{-7} m^2/Vs$ [18]. The relative permittivity of all oil types in this study is 3.2. Using these values, and the Ohmic conductivities measured at low field, the saturation voltage (V_s) is calculated as shown in Table 2.

Fig. 4 shows the conduction current for oil A with various gap settings. V_s depends apparently on the gap separation. For small gap, V_s is generally low and it increases with gap separation. It is clear from Fig. 4 that the measured current density (symbols) follows initially Ohmic and then injected current density. The theoretical current density (solid lines) have been computed based on equations in Table 1.

The inset of Fig. 4 shows the characteristics of current density versus the applied field at low field. Interestingly, the data points of the various electrode gaps lied onto one straight line on the semi-log plot shown in the insert for fields below the saturation ($E_S = V_s/d$). In this region, the conduction is considered purely ohmic.

3.2. Distribution of field in different conduction regimes

The combined effects of electrode gap and oil type on the field distribution are shown in Figs. 5 and 6. The distortion rate of the

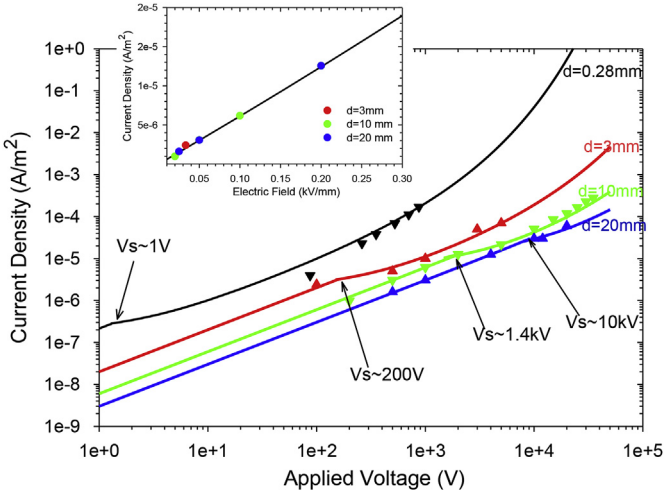

Fig. 4. Experimental current-voltage characteristics corresponding to oil A with different electrode gaps. The inset shows the variation of current density with the electric field at different electrode gaps. Oil B and oil C also show similar behaviour.

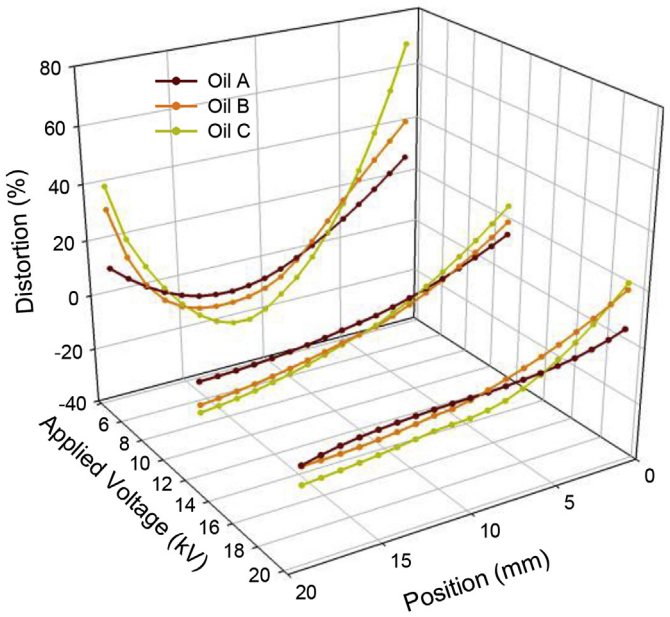

Fig. 5. The relative field distortion at three different applied voltages (4 kV, 12 kV, 20 kV) for oil A, B and C over 20 mm oil gap.

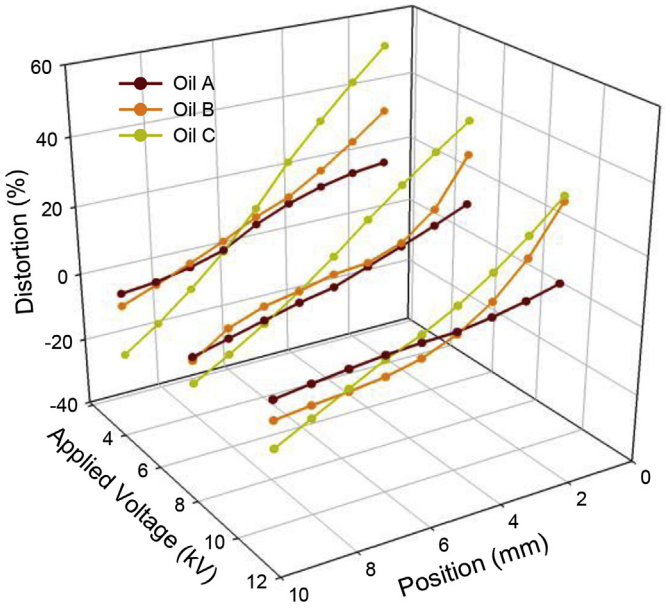

Fig. 6. The relative field distortion at three different applied voltages (2 kV, 6 kV, 10 kV) for oil A, B and C over 10 mm oil gap.

electric field between the electrodes was calculated using equation (3):

$$D = \frac{E - E_{ave}}{E_{ave}} \times 100\% \quad (3)$$

where D is the distortion rate, E is the measured field and E_{ave} is the value of the average applied electric field.

In Fig. 5, the electrode gap was set to 20 mm and three different voltage levels (4 kV, 12 kV and 20 kV) were applied to probe the field distribution in various regimes. For 20 mm electrode gap, 4 kV lies below V_s. Therefore, dissociation of impurity in bulk oil is the source of charge carriers. Charge dissociation causes heterocharge formation which tends to increase the magnitude of the electric field near electrodes resulting in a symmetrical U shaped electric field distribution [6]. These results are in good consistency with the Ohmic current-voltage characteristics revealed experimentally for large oil gap under low voltages.

With the applied voltage increased to 12 kV and 20 kV, an asymmetric field distribution was observed. The field intensity decreases quasi-linearly from cathode to anode, which implies the presence of positive ions in the oil gap, "injected" through carrier exchange at the liquid metal interface. This is in line with the measured current-voltage characteristics for a high field($V > V_s$) where the injection is the major contributor for the total conduction current.

Similar field distribution was reported in the pioneering work by Uno Gävert et al. for transformer oil under electrode gap of 19 mm [6]. It was reported that at low field (0.1–0.3 kV/mm) the electric field as a function of position in the oil gap follows a parabolic shape, which can be well modelled with the ion drift model (without injection) [6]. Interestingly, at a moderately high field of ~1 kV/mm, a different type of field distribution emerges, i.e., the field increases monotonically from the positive electrode to the negative electrode. This type of field distribution was explained in Ref. [6] by considering a mobility disparity between positive and negative ions by a factor of four. However, more recent studies [18,19] indicate that such polarity dependent disparity in ionic mobilities does not exist. In our present study, the transition from symmetrical to asymmetrical field distribution can be explained readily by field-dependent charge injection from the electrodes as described in Ref. [15].

Fig. 6 shows the field distribution with the electrode gap reduced to 10 mm. Within the voltage range under study, the electric field is found to be low near the positive electrode and high near the ground electrode. This field distribution implies the injection of positive ions. This is in good agreement with the current-voltage characteristics curve measured at 10 mm electrode gap shown in Fig. 4, which suggests unipolar carrier injection for voltages above 1.4 kV.

For the three oil types investigated (Figs. 5 and 6), there is an apparent correlation between the degree of field distortion, the type of oil and electrode gap separation. Oil C shows the strongest field enhancement among the three types of oil. The increase of conductivity due to moisture and contaminant appears to make the electric field distribution even more non-uniform. In addition, it is clearly seen that field distortion reduces with the reduction of electrode gap separation.

3.3. Field mapping along solid-liquid interface

In this regard, the electric field distribution was measured at nine locations for geometries A and B as marked in Fig. 3b and c under an applied voltage of +15 kV. As shown in Fig. 7, under DC grading, the electric field intensity across the interface from position 0–5 mm is higher than the remaining portion of the interface because the volume resistivity ratio of epoxy to oil is as high as several tens or over one hundred. For this reason, most of the DC voltage is distributed across epoxy. Geometry B shows higher field intensity than geometry A due to better shielding effect as shown in Fig. 3c.

3.4. Effect of applied voltage polarity

HVDC subsea system could be subjected to bipolar voltage waveforms either by design or during fault transients. Therefore, it is important to study the behaviour of the solid-liquid insulation system for both positive and negative WM chambers. Finite Element Method (FEM) simulation of the field distribution along the solid-oil interface for geometry A and B can be found in Fig. 7b (epoxy dielectric constant = 4.2 and conductivity $\sim 10^{-14}$ S/m; oil dielectric constant = 3.2 and conductivity $\sim 10^{-12}$ S/m). The contours in the insert represent equipotential lines.

While the overall field distribution from the simulation can be found in general agreement with the measurement results as shown in Fig. 7a, the deviation of magnitudes of electric fields particularly near the electrodes supports once again the presence of positive ions in synthetic

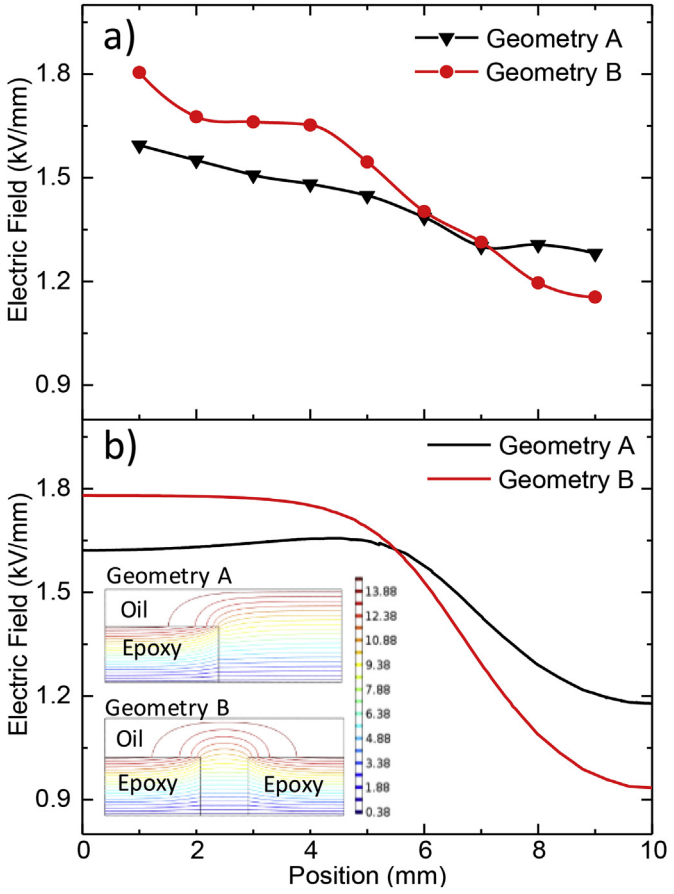

Fig. 7. The electric field intensity measured (a) and simulated (b) across the interface for geometries A and B under +15 kV.

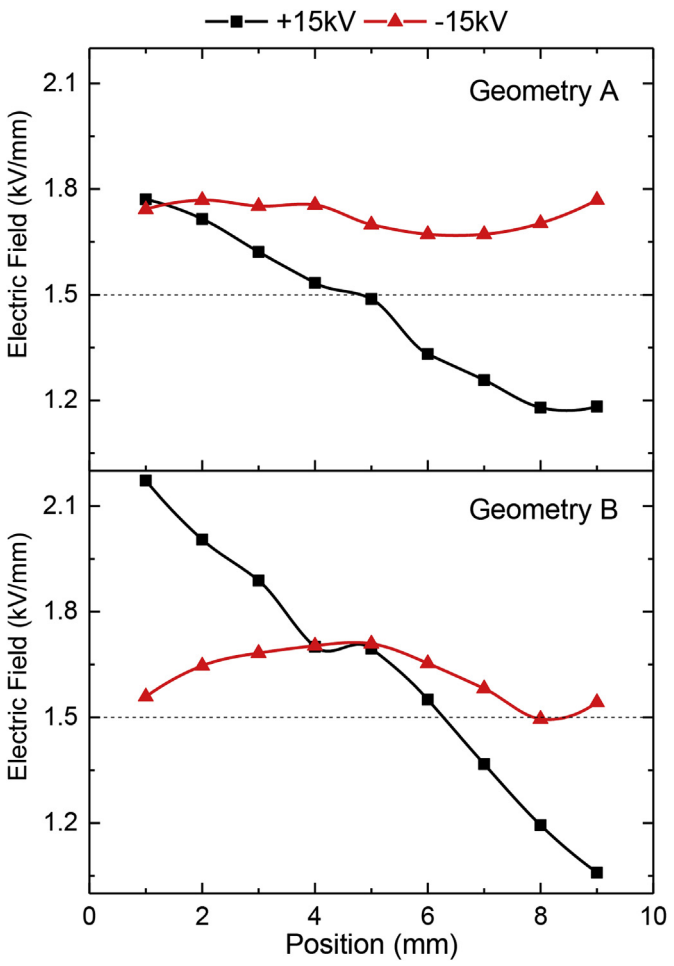

Fig. 8. Kerr electro-optics measurement showing the effect of the positive and negative applied voltages for geometries A and B with oil type B. Similar behaviour is observed for oil types A and C.

ester oil under these testing conditions. Such field modification due to the presence of positive ions can be observed more clearly with the refined studies involving the effects of polarities, as shown in Fig. 8. For geometry A under DC+, the electric field magnitude increases nearly-linearly from the positive electrode to the ground electrode. However, it is not seen for geometry A under DC-. According to the FEM simulation shown in Fig. 7b, the field along the solid-liquid interface shall stay relatively flat near the "grounding" side and decreases slowly over the transition of solid-oil to pure oil gap to another plateau. This "Z-stair case" field distribution is due to the "shielding" effect of solid dielectric with a much higher electric resistivity than oil. With the presence of positive ions in the oil, this "Z-stair case" field distribution will be modified into "nearly-linear" under positive polarity and "nearly-uniform" under negative polarity, respectively. This effect can be observed for both geometry A and geometry B, as shown in Fig. 8. Furthermore, the average measured fields for geometry B are in good agreement with the voltage applied, i.e., 15 kV over 10 mm gap (1.5 kV/mm), while the average measured fields for geometry A appear higher. This is due to the fact that geometry B as shown in Fig. 3c possesses reflection symmetry and, as a result, the field along the solid-oil interface has no tangential field components. However, this is not true for geometry A where the measured field by Kerr optics is generally higher due to the existence of tangential field components.

3.5. Effect of thickness of dielectric solid on field distribution in the solid-liquid system

In this section, the effect of epoxy plaque thickness on the electric field magnitude is studied. Epoxy plaque with 6 mm, 4 mm and 2 mm thickness was placed on the ground electrode. When a DC voltage is applied, the time variation of an electric field at marked locations was measured as shown in Fig. 9a.

Fig. 9b to d show the electric field distribution in the oil at steady-state under different oil gaps. From the results, there is a significant change in electric field distribution with the change of the width of the oil gap. When the epoxy thickness is decreased from 6 mm to 2 mm (or the oil gap increases from 4 mm to 8 mm), the steady state field value increases at every measuring point. As it will be shown in the next section, this field mapping gives a reasonable picture of stress levels, useful for dimensioning purpose of solid-liquid gap spacing. In addition, for positive voltage the magnitude of the electric field increases in the middle measuring points of the oil gap. However, in the measuring points placed close to the anode, the field decreases. This is due to the unipolar injection of positive charges from the positive electrode as explains in section 3.2. This leads to the formation of homocharges near the anode which tends to decrease the magnitude of the electric field. However, for the case of negative voltage, the presence of positive ions near the negative electrode leads to the formation of heterocharges which tends to increase the magnitude of the electric field from the surface of the epoxy all way to the vicinity of the electrode.

4. Electric field control in actual wet mate connector

4.1. Steady state study

Based on the aforementioned studies, we investigated the electric field distribution in a representative WM connector with only a single

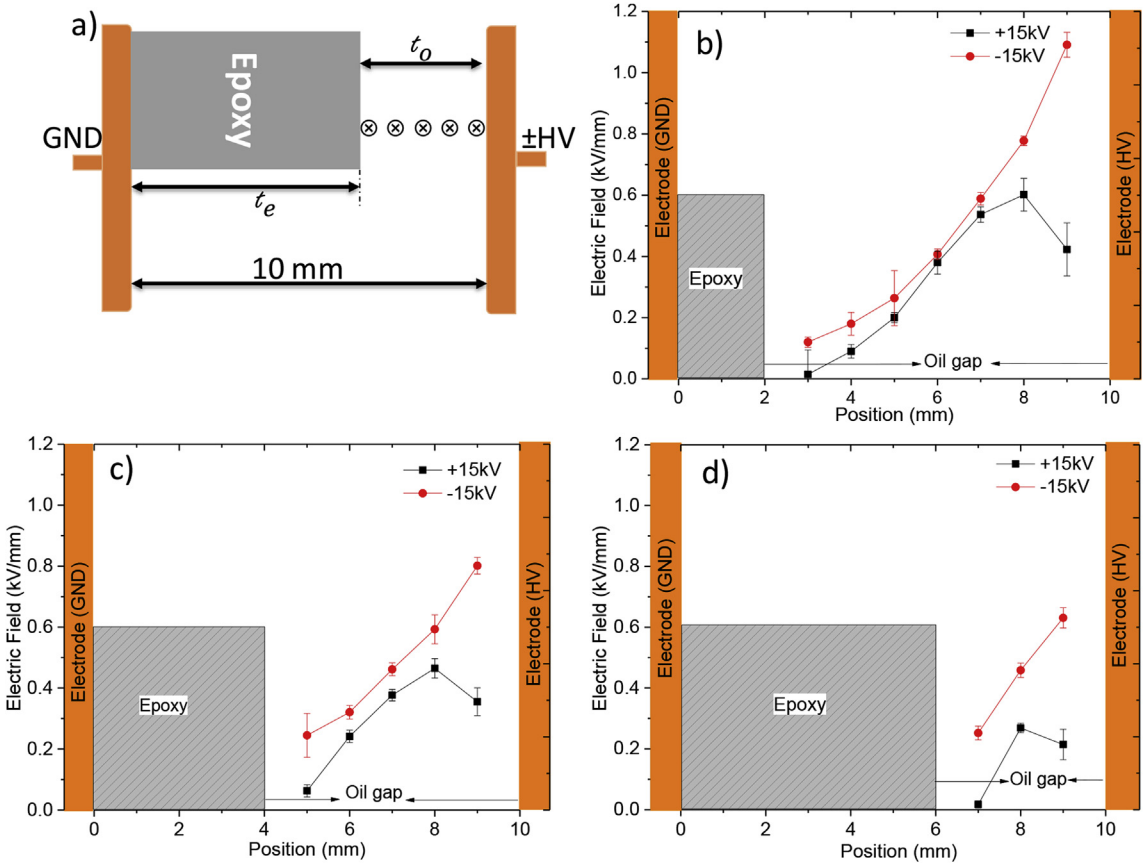

Fig. 9. a) Geometry A with variable epoxy thickness (t_e) and variable oil thickness (t_o) b) Electric field distribution measured in oil gap space at quasi steady-state with t_e = 2 mm epoxy c) t_e = 4 mm epoxy d) t_e = 6 mm epoxy. The error bars represent the standard deviation of the quasi-steady state measurements.

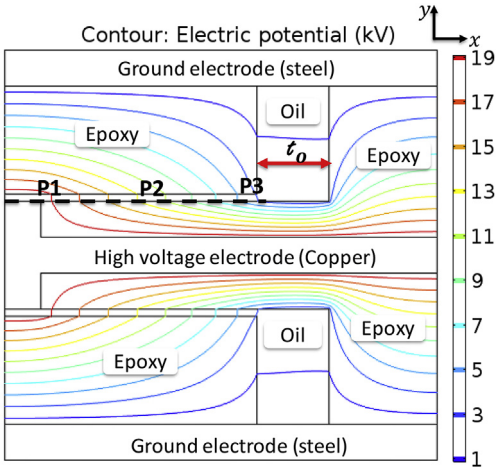

Fig. 10. DC field distribution in WM chamber. The contours represent equi-potential lines, and denser contours indicate higher electric fields. The electric field is completely expelled from oil since the conductivity of oil is about two orders of magnitude higher than that of epoxy. The field along the dashed line is plotted in Fig. 11.

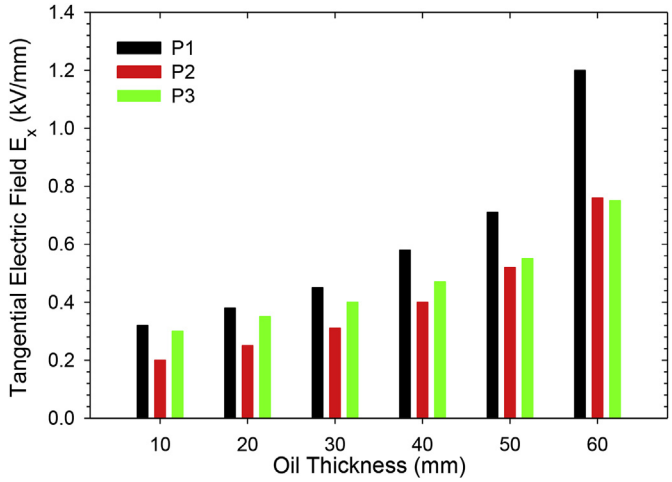

Fig. 11. Maximum tangential electric field (E_x) across the interface locations P1, P2 and P3 for different oil thickness.

conductor rated at voltage of $20kV$. The electric field across the interface is computed at three points of interest (P1, P2, P3) as shown in Fig. 10. Point P1 is the triple point junction, where the epoxy and the oil meet at the electrode surface. Point P2 is the middle point of oil channel and point P3 is at the edge of the oil channel. It is worth noting that the study focused on electric fields in the oil along the interfaces. Even though the electric field in the epoxy may be higher, it is not a major concern due to the high dielectric strength of the epoxy. Fig. 11 summarizes the maximal tangential field at these three locations with varying oil thickness (t_0).

There is a significant change of electric field distributions with the change of the width of the oil gap thickness. Point P1 shows a maximum field stress regardless of the oil thickness. Minimizing the field at the triple point junction is desirable since it is directly related to the possible initiation of discharges that can lead to flashover and failure of the chamber. Reducing the oil gap width remarkably reduces the field stresses along the interface while increasing oil channel width enhances the field. This supports the experimental result presented in sections 3.2

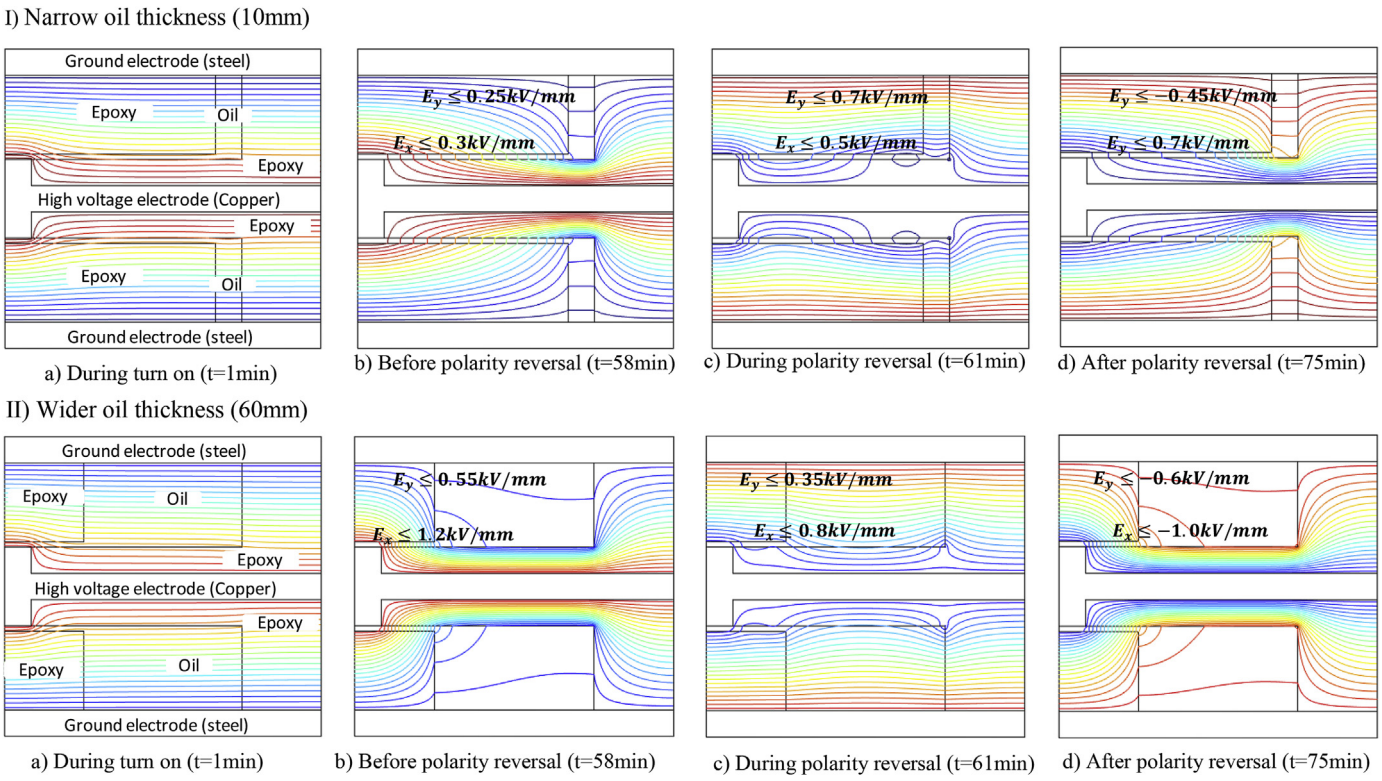

Fig. 12. The electrical stress distribution under polarity reversal in a WM chamber. The contours represent equipotential lines, and denser contours indicate higher electric fields. The electrical stress concentration mainly happens on solid insulation and around the solid/oil interface region. In terms of DC insulation design, the stress concentration in these focused areas shall be minimized. The distribution of equipotential lines along the solid-liquid interface is uniform for the narrow oil thickness compared with wider oil thickness. This indicates a uniform and low tangential electric field distribution for the case of narrow oil thickness. The equipotential lines are much denser along epoxy oil interface for the wider oil thickness, which indicates stress concentration in these regions.

& 3.5, where the field is measured at different oil gaps. The accumulation of space charge near electrode with wider oil gap causes field enhancement. Therefore, short oil thickness is recommended.

4.2. Polarity reversal study

In order to analyse the transient response of the connector qualitatively, the electric field distributions during and after the polarity reversal events have been numerically modelled. Polarity reversal represents an extreme case of transient response. Analysing this case can also provide information regarding the response under turn on and turn off process.

The connector is initially stressed with $+\ 20kV$ DC for 60min. The polarity reversal from $+\ 20kV$ to $-\ 20kV$ takes place over a period of 2min [20]. Then the voltage is kept at $-\ 20kV$ for the next 60min. Fig. 12 illustrates the overall field distribution in the WM chamber during and after polarity reversal. When the voltage is turned on, the electric field is instantaneously established between the center conductor and the conductor at the ground potential. The electric field distribution follows capacitive grading (Fig. 12a) within a very short time after the voltage is applied because the electric charges have not yet responded to the electric field. At this stage, the electric field distribution is relatively uniform due to the fact that relative permittivity of oil (3.2) and epoxy (4.2) are very similar to AC field grading. Then the charge distribution starts to evolve in response to this established electric field and reach quasi steady-state, in which the electric field follows resistive grading (Fig. 12b). During polarity reversal (Fig. 12c), the field distribution shows mixed features of capacitive and resistive graded fields. At longer times after the polarity reversal (Fig. 12d), the field distribution slowly relaxes to the steady-state DC field along the opposite direction. The maximum field level along the epoxy-oil interface in x-direction can be reduced to below 0.5 kV/mm by reducing the oil thickness (Fig. 12I oil thickness of 10 mm). On the other hand, the maximum interfacial field strength along the y-direction is controlled to below 0.7 kV/mm under both steady state and transient conditions. For the case of wider oil gaps (Fig. 12II oil thickness of 60 mm), the tangential field is > 1 kV/mm. Such field computation shall provide a quantitative basis for the design trade-off study for WM DC connector.

5. Conclusion

Using the current-voltage and Kerr electro-optic measurements, the present study analyzed the field distribution in oil and oil/epoxy hybrid insulation system under DC-related electrical conditions for wet-mate connectors, with the following major findings:

(i) There are transitions in the electric field distribution in oil insulation employed in WM DC connectors in accordance with the conduction regimes. For applied voltage less than the saturation voltage (V_s), conduction is dominated by ion dissociation in the oil bulk. Such Ohmic conduction will lead to the formation of heterocharges giving symmetrical field distribution. With applied voltage higher than saturation voltage (V_s), this bulk conduction will transit to extrinsically dominated conduction with carriers injected through liquid-electrode interfaces. Under such carrier injection mechanism, the corresponding field distribution becomes asymmetrical.

(ii) Such field distortions are fully investigated by considering effects of electrode configuration, gap separation, polarity, oil type, moisture and contaminants, and further extended to hybrid solid-liquid insulations particularly along the solid-liquid interfaces.

(iii) In hybrid solid-liquid insulations, for both DC polarities, electric fields particularly near the electrodes are distorted due to the presence of positive ions in the oil gap. Such field distortion is seen enhanced with the presence of deionized water and instant ocean water contaminants. However, due to the high contrast of volume resistivity between epoxy and oil, most of the DC voltage is distributed across epoxy. It is suggested that shielding effect can be leveraged for mitigating the tangential field concentration along the solid-liquid interface.

(iv) These findings were employed in a FEM modelling study of a representative WM DC connector to tailor the design of solid-liquid interfaces for low field distortion under quasi steady-state and polarity reversal. The electric field distortion can be designed to be very low provided that the separation between the solid barriers in the hybrid insulation structure be narrow.

Studies presented in this work are expected to provide inputs to promote in-depth understanding of solid-liquid insulation system for the safe design of Wet-Mate DC connectors.

Acknowledgments

Funding for this work is provided by RPSEA through the “Ultra-Deepwater and Unconventional Natural Gas and Other Petroleum Resources” program authorized by the U.S. Energy Policy Act of 2005. RPSEA (www.rpsea.org) is a nonprofit corporation whose mission is to provide a stewardship role in ensuring the focused research, development, and deployment of safe and environmentally responsible technology that can effectively deliver hydrocarbons from domestic resources to the citizens of the United States. RPSEA, operating as a consortium of premier U.S. energy research universities, industry, and independent research organizations, manages the program under a contract with the U.S. Department of Energy's National Energy Technology Laboratory.

The authors would like to thank JoAnne Ronzello and Robert Fleming for help with the experiment.

Appendix A. Supplementary data

Supplementary data related to this article can be found at http://dx.doi.org/10.1016/j.elstat.2018.06.001.

References

[1] I. Østergaard, A. Nysveen, T. Romanisko, MECON: a high voltage subsea connector, The Proceedings of Offshore Technology Conference, 1999 OTC 10948.
[2] S. Rocke, Subsea power transfer, what is the challenge, SPE Applied Technology Workshop, Technology for the Next Generation Subsea System, Oslo, Norway, Feb. 11, 2003.
[3] GE Vetco Gray, MECON WM-I and II, Product Information Sheet.
[4] GE Global Research Report, MSDC Electrical System for Deepwater Subsea Process, Contract No. 08121-2901-01 (2013).
[5] GE Global Research Report, Subsea High Voltage Direct Current Connectors for Environmentally Safe and Reliable Powering of UDW Subsea Processing, Contract No. 12121-6302-01 (2015).
[6] U. Gafvert, A. Jaksts, C. Tornkvist, L. Walfridsson, Electrical field distribution in transformer oil, IEEE Trans. Electr. Insul. 27 (1992) 647–660.
[7] M. Tefferi, M. Ghassemi, C. Calebrese, Q. Chen, Y. Cao, Characterization of solid-liquid interface for wet-mate subsea HVDC connectors, Annu. Rep. Conf. Electr. Insul. Dielectr. Phenom, 2016, pp. 735–738.
[8] M. Tefferi, M. Ghassemi, C. Calebrese, Q. Chen, Y. Cao, Characterization of solid-liquid interface in a wet-mate subsea HVDC connector, Jicable-HVDC’17, Int. Symp. HVDC Cable Systems, Dunkirk, France, Nov.20-22, 2017, pp. 1–6.
[9] T. Maeno, Y. Nonaka, T. Takada, Determination of electric field distribution in oil using the Kerr-effect technique after application of DC voltage, IEEE Trans. Electr. Insul. 25 (1990) 475–480.
[10] K. Nakamura, K. Kato, H. Koide, Y. Hatta, H. Okubo, Fundamental property of electric field in rapeseed ester oil based on Kerr electro optic measurement, IEEE Trans. Dielectr. Electr. Insul. 13 (2006) 601–607.
[11] A. Alj, A. Denat, J.P. Gosse, B. Gosse, I. Nakamura, Creation of charge carriers in nonpolar liquids, IEEE Trans. Electr. Insul. 20 (1985) 221–231.
[12] A. Denat, Conduction and breakdown initiation in dielectric liquids, IEEE Int. Conf. Dielectric Liquids (ICDL) (2011) 1–11.
[13] F. Pontiga, A. Castellanos, Electrical conduction of electrolyte solutions in nonpolar liquids, IEEE Trans. Ind. Appl. 32 (1996) 816–824.
[14] A. Denat, B. Gosse, J.P. Gosse, Ion injections in hydrocarbons, J. Electrost. 7 (1979) 205–225.
[15] A. Denat, B. Gosse, J.P. Gosse, Electrical conduction of solutions of an ionic surfactant in hydrocarbons, J. Electrost. 12 (1982) 197–205.
[16] N.J. Felici, A tentative explanation of the voltage-current characteristics of dielectric liquids, J. Electrost. 12 (1982) 165–172.
[17] J.C. Fillipini, Recent progress in Kerr cell technology, physical considerations, J. Phys. D Appl. Phys. 8 (1975) 201–213.
[18] Y. Jing, I.V. Timoshkin, M.P. Wilson, M.J. Given, S.J. MacGregor, T. Wang, Dielectric properties of natural ester, synthetic ester midel 7131 and mineral oil Diala D, IEEE Trans. Dielectr. Electr. Insul. 21 (2014) 644–652.
[19] L.J. Yang, S.M. Gubanski, Y.V. Serdyuk, J. Schiessling, Dielectric properties of transformer oils for HVDC applications, IEEE Trans. Dielectr. Electr. Insul. 19 (2012) 1926–1933.
[20] W. G. B1.32, Recommendations for testing DC extruded cable systems for power transmission at a rated voltage up to 500 kV, Cigre TB 496 (April 2012) 1–36.